Highlights of Spanish Astrophysics XI, Proceedings of the XV Scientific Meeting of the Spanish Astronomical Society held on September 4–9, 2022, in La Laguna, Spain. M. Manteiga, L. Bellot, P. Benavidez, A. de Lorenzo-Cáceres, M. A. Fuente, M. J. Martínez, M. Vázquez- Acosta, C. Dafonte (eds.), 2023

Martian CO profiles from the solar occultation experiment of NOMAD on board TGO.

Modak, A.[1], López-Valverde, M.A.[1], Brines, A.[1], Stolzenbach, A.[1], Funke, B.[1], González-Galindo, F.[1], Liuzzi, G.[2,5] Aoki, S.[2,3] Thomas, I.[3] Villanueva, G.[2] Erwin, J.[3] Lopez-Moreno, J.J. [1] Yoshida, N.[6] Grabowski, U.[7] Forget, F.[8] Daerden, F.[3] Ristic, B,[3] Belucci, G,[9] Patel, M.[10] Trompet, L.[3], and Vandaele, A.C.[3]

[1]Instituto de Astrofísica de Andalucia, Granada, Spain
[2]NASA Goddard Space Flight Center, USA
[3]Belgian Royal Institute for Space Aeronomy, Brussels, Belgium
[4]Japan Aerospace Exploration Agency (JAXA), Japan
[5]American University, Washington DC, USA
[6]Graduate School of Science, Tohoku University, Sendai, Japan
[7]Karlsruhe Institute of Technology, Institute of Meteorology and Climate Research, Karlsruhe, Germany
[8]Laboratoire de Météorologie Dynamique, IPSL, Paris, France
[9]Institute for Space Astrophysics and Planetology, Italy
[10]Open University, Milton Keynes, UK

Abstract

Carbon monoxide is one of the important minor species in the Martian atmosphere due to its role in the photochemical stability of the CO_2 atmosphere and can also be used as a dynamical tracer. The SO spectrometer onboard the Trace Gas Orbiter (TGO) scans the Martian limb in the infrared provides transmittances with fine vertical sampling ($\sim$ 1km). In the spectral region, the sounding of CO is found to be reliable due to its strong and well separated absorption lines. Here, we present the retrieval scheme for CO from the solar occultation observation. Our scheme obtains density profiles up to 100 km with a vertical resolution better than 5km and errors below 15%. The observations for the last two seasons of Mars Year 34 (MY34, April 2018 - March 2019) are analyzed here. We found important results such as a strong depletion of CO density during the global dust storm (GDS) and a clear dynamical influence of global Hadley circulation on the CO distribution.

1 Introduction

Untill the arrival of TGO, detailed systematic mapping of the Martian CO density and its variation in the vertical was essentially absent. The instrument NOMAD (Nadir and Occul-

tation for MArs Discovery) and ACS (Atmospheric Chemistry Suite) have proved themselves as successful instruments in terms of measuring atmospheric trace gases. The CO retrieved from the mid-infrared (MIR) channel of ACS showed a depletion in CO density during the global dust storm (GDS) of MY 34 [13]. A detailed quantitative comparison study based on the retrieved profiles from the ACS MIR, NIR, and TIRVIM can be found in [3]. Here, we present vertical profiles of CO retrieved from the measurements recorded by NOMAD solar occultation (SO) for the first year of TGO observations from April 2018 to March 2019, for the first time. This covers the last two seasons of MY 34 with fine latitudinal coverage. An extended version of this work can be found in a recently submitted manuscript [12].

2 The NOMAD Solar Occultation Channel

NOMAD is a suite of three spectrometers SO (Solar Occultation Channel), LNO(Limb and Nadir Occultation) and UVIS(The Ultraviolet and Visible Spectrometer) [16] onboard TGO. In this study, we only have used the SO observations. The SO spectrometer operates in the spectral range of 2.2-4.3μ m with a nominal resolving power $\sim$ 20,000. The spectrometer is primarily composed of an echelle grating in Littrow configuration which means the incident, the reflected and the blaze angles are equal. The other important components of the spectrometer are the detector, parabolic mirrors, and the Acousto Optical Tunable Filter (AOTF). The AOTF, controlled by radio frequency, works as a bandpass filter and should ideally, allow only one selected diffraction order to fall onto the detector. In practice, AOTF introduces contamination from the adjacent diffraction orders due to which we only process the spectra in selected microwindows (MWs)(see [12] for details).

The components of the SO spectrometer such as the detector, the AOTF, and the grating are characterized by numerical parametric functions. These functions are respectively, the Instrumental Line Shape (ILS), AOTF transfer function, and the blaze function. The blaze function is taken from [8] and the ILS and AOTF are determined by our team in collaboration with other NOMAD teams which is described in [17]. The AOTF transfer function has been further finetuned by our retrieval method as described in [12]. These parameters are essential for theoretical simulation of the SO spectra and have been convolved within forward model called KOPRA(Karlsruhe Optimized and Precise Radiative transfer Algorithm)[14] to determine the incoming solar radiation received by the spectrometer. Both the preprocessing and the inversion which are described next make use of the line-by-line forward model KOPRA.

3 Preprocessing and Inversion

The SO spectra used for this study are Level 1 calibrated data which provides atmospheric transmittances along with the measurement noises at all altitudes in every scan or orbit. The left panel of Figure 1 shows an example of these spectra for a given scan. The spectra clearly suffer from several residual calibration effects like spectral bending and shift. As an initial step, we clean these calibration issues before feeding the spectra into our retrieval scheme. We call this internal step preprocessing. The preprocessing is described in detail in [9, 1, 12].

The right panel of Figure 1 shows the cleaned/preprocessed spectra which are corrected for the spectral bending and the spectral shift.

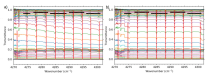

Figure 1: Example of our cleaning method applied to diffraction order 190 in one specific scan. Panel (a), all the original spectra (Level 1 calibrated transmittances) taken in this scan, showing clear bending effects and spectral shifts. Panel (b), spectra after cleaning.

Here we describe, in brief, the working principle of our retrieval scheme managed by a Retrieval Control Program (RCP) which performs a global fit (spectra at all altitudes) iteratively. The preprocessing and the retrieval scheme are common to our group targetting other atmospheric quantities such as temperature [10], water vapor [2], and aerosols [15]. The RCP runs KOPRA iteratively keeping the CO, continuum, and spectral shift as free parameters and compares the simulated spectra with the cleaned measured spectra until the best fit is obtained. The continuum is simulated by a spectrally constant transmittance level, adjusted to account for the impact of aerosol absorption. The goodness of our fit is characterized by $\boldsymbol{\chi^2}$ value obtained from the global fit method. For a more detailed description of this retrieval scheme the reader should refer to [12].

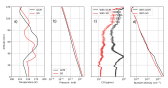

Figure 2: The effect of the reference thermal structure on the retrieved CO.

Retrieved CO values are highly dependent on the *a priori* temperatures [7]. To quantify the effect of temperature, we use simulated and retrieved climatologies[9] in the example depicted in Figure2. Figure2 shows two sets of atmospheric quantities; pressures, temperatures, mixing ratios, and number densities. Pressures and temperatures are referring to the apriori climatologies while the mixing ratios and the number densities are the results of the retrievals with those climatologies. The black curves are corresponding to the GCM scenario while the red curves are to the retrieval with SO T/P. The differences in CO number densities and the mixing ratios are indicating the sensitivity of CO retrievals on the apriori climatologies. This demonstrates that it is very important to use realistic temperatures profiles from a previous inversion from the same scan.

4 CO profiles and Variability

Above 60 km CO is produced by the photolysis of the CO_2 and the variability in these mesospheric altitudes is dominated by the production and atmospheric circulation while the lower atmosphere (below 60 km) is dominated by the loss of CO[6, 4, 11]. This inspires us to describe the CO variability of these two altitude regions separately with the help of an arbitrary marker fixed at the orange iso contour representing a CO VMR value of 2500 ppm (see Figure 3). There are two different seasons where the upper atmospheric CO distribution reflects the Martian dynamical behavior. During the northern autumn equinox (L_S = 160° - 180°) when the two Hadley cells extend from the equator to the high latitudes over both the hemispheres, CO enriched air from the low latitude regions most likely to downwell over the high latitude regions. Thus the increase in the CO mixing ratio is observed over the high latitudes during this period. During the southern soltice in the period $L_S \sim 280°$, the reference orange contour seems to reach down to altitudes near 60 km over the northern hemisphere (NH) whilst over the southern hemisphere (SH), this contour seems to retract towards altitudes above 80 km. This kind of upper atmospheric CO distribution points towards an interhemispheric circulation from SH to NH. The behavior of CO distribution in the lower atmosphere is mostly controlled by its loss. The loss is apparent during the onset of the GDS when CO is depleted due to the rise in water content of the atmosphere. This loss again becomes dominant during the southern summer but in this period the depletion might be due to a combined effect of the release of water vapor and CO_2 from the southern polar cap due to their annual sublimation. The release of CO_2 increases the total atmospheric mass thus depleting the CO mixing ratio.

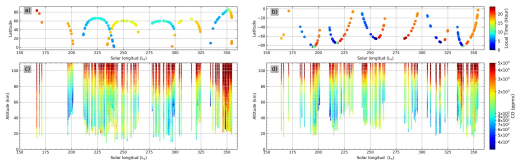

Figure 3: All CO profiles retrieved for this study. The upper panels ((a) and (b)) show the L_S-latitude distribution of the dataset used, with the colors on scale indicating the localtime. The bottom panels show L_S-altitude distribution of the CO profiles corresponding to the location shown in the top panels.

Figure 4 shows the latitudinal distribution of the CO profiles for small L_S periods. The left-hand panels of the Figure 4 show the retrieved CO distribution for fixed L_S periods corresponding to the northern equinox and southern summer while the right-hand panels

(panels (b),(d),(f) & (h)) show the corresponding CO distribution from the GCM simulations. The GCM simulated CO distributions are shown in order to illustrate the departure from apriori and to predict possible dynamical effects. During the northern equinox, the Martian dynamics is dominated by the two Hadley cells extending from the equatorial regions to the high latitude regions. The SO observations, in panel (a) suggest an increase in the low altitude CO abundance over high latitude due to the hemispheric Hadley cells which are also depicted in panel (b). At the beginning of the southern summer(panels (c) & (d)), there seems to be an increase in CO density in the upper altitudes which is probably a result of the increased photodissociation due to the increased solar insolation. The next panel (e) shows a globally developed interhemispheric Hadley cell which is not apparent in the simulation panel (f). According to our results, and despite the patchy maps obtained, it seems that the Hadley cell originates over the southern latitude $> 40°$S and downwells over the 60°N.

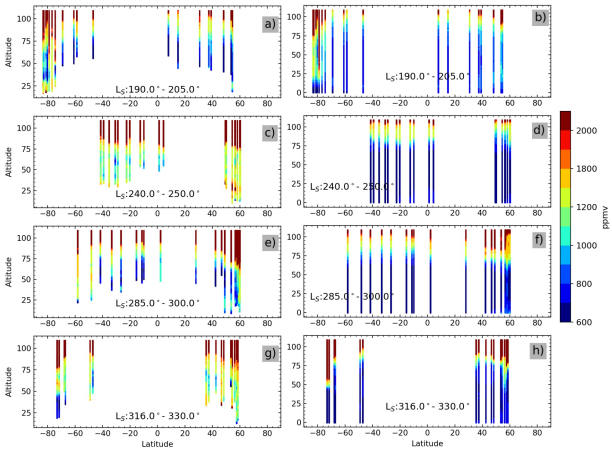

Figure 4: Latitudinal distribution of the retrieved, on the left panels ((a), (c), (e), & (g)) and GCM-simulated CO profiles on the right panels ((b),(d),(f), & (h)) Each panel corresponds to a fixed L_S period.

Acknowledgments

The IAA/CSIC team acknowledges financial support from the State Agency for Research of the Spanish MCIU through the 'Center of Excellence Severo Ochoa' award for the Instituto de Astrofsica de Andaluca (SEV-2017-0709) and funding by grant PGC2018-101836-B-100 (MCIU/AEI/FEDER, EU) and PID2019-110689RB-I00/AEI/10.13039/501100011033 Grant PRE2019-088355 funded by MCIN/AEI/ 10.13039/501100011033 and by 'ESF Investing in your future'. F.G.G. is funded by the Spanish Ministerio de Ciencia, Innovacion y Universidades, the Agencia Estatal de Investigacion and EC FEDER funds under project RTI2018-100920-J-I00.

References

[1] Brines, A., López-Valverde, M. A., Stolzenbach, A., Modak, A., Funke, B., Galindo, F. G., ... & Vandaele, A. C., 2022, JGR Planets, e2022JE007273

[2] Brines, A., López-Valverde, M. A., Stolzenbach, A., Modak, A., Funke, B., Galindo, F. G., ... & Bellucci, G., 2022, In Seventh International Workshop on the Mars Atmosphere: Modelling and Observations, (p. 2402)

[3] Fedorova, A., Trokhimovskiy, A., Lefèvre, F., Olsen, K. S., Korablev, O.,Montmessin, F., . . . others, 2022, JGR Planets, e2022JE007195

[4] González-Galindo, F., Forget, F., López-Valverde, M., Angelats i Coll, M., & Millour, 2009, JGR Planets, 114(E4)

[5] Gordon, I. E., Rothman, L. S., Hill, C., Kochanov, R. V., Tan, Y., Bernath, P. F.,. . . others, 2017, JQSRT, 203 , 3–69

[6] Krasnopolsky, V. A., 1995, JGR Planets, 100 (E2), 3263–3276

[7] Krasnopolsky, V. A., 2003, JGR, Planets, 108 (E2)

[8] Liuzzi, G., Villanueva, G. L., Mumma, M. J., Smith, M. D., Daerden, F., Ristic, B., . . . others, 2019, Icarus, 321 , 671–690

[9] López-Valverde, M.-A., Funke, B., Brines, A., Stolzenbach, A., Modak, A., Hill, B., . . . others 2022, JGR: Planets, e2022JE007278

[10] López-Valverde, M. A., Funke, B., Brines, A., Modak, A., Stolzenbach, A., Gonzalez-Galindo, F., ... & Vandaele, A. C., 2022, In Seventh International Workshop on the Mars Atmosphere: Modelling and Observations, (p. 1406)

[11] Modak, A., Sheel, V., & Lefèvre, F., 2020, PSS, 181

[12] Modak, A., López-Valverde, M. A., Funke, B., Brines, A., Stolzenbach, A., Gonzalez-Galindo, F., & others, 2022, JGR Planets, submitted

[13] Olsen, K., Lefèvre, F., Montmessin, F., Fedorova, A., Trokhimovskiy, A., Baggio, L., & others, 2021, Nature, Geoscience, 14(2), 67–71

[14] Stiller, G. P., 2000

[15] Stolzenbach, A., Lopez Valverde, M. A., Brines, A., Modak, A., Funke, B., Gonzalez-Galindo, F., ... & Aoki, S., 2022, In Seventh International Workshop on the Mars Atmosphere: Modelling and Observations, (p. 2206)

[16] Vandaele, A. C., Lopez-Moreno, J.-J., Patel, M. R., Bellucci, G., Daerden, F., Ristic,B., . . . others, 2018,Space Science Reviews, 214 (5), 1–47

[17] Villanueva, G. L., Liuzzi, G., Aoki, S., Stone, S. W., Brines, A., Thomas, I. R., . . .others, 2022 Geophysical Research Letters, 49 (12), e2022GL098161